Hybrid Observer Combining Measurements of Different Fidelities ⋆

Astrid H. Brodtkorb * **Andrew R. Teel** ** **Asgeir J. Sørensen** *

* *Centre for Autonomous Marine Operations (NTNU AMOS), Department of Marine Technology, Norwegian University of Science and Technology (NTNU), Otto Nielsens vei 10, 7491 Trondheim, Norway (e-mails: astrid.h.brodtkorb@ntnu.no, asgeir.sorensen@ntnu.no*

** *Department of Electrical and Computational Engineering, University of California Santa Barbara, CA USA (e-mail: teel@ece.ucsb.edu)*

Abstract: A signal-based hybrid observer combining measurements of different fidelities is proposed for position and velocity estimation of marine vessels. The concept assumes that noisy position measurements are available only sporadically at a non-constant sampling rate. Predictions of position between the samples are provided by integrating acceleration measurements, which are available at a high rate (approximated to be continuous sampling). Estimates with smaller variance are computed by averaging multiple observer copies of the position. This work is a continuation of the observer proposed in Brodtkorb et al. (2015). The main contributions of this paper is extending the observer to the more realistic scenario where linear velocity and angular acceleration measurements are not available. A simulation study showed that the observer performed well in closed loop with a controller conducting dynamic positioning operations of a marine vessel.

Keywords: Observers, hybrid systems, dynamic positioning, sensor fusion

1. INTRODUCTION

Observers are important components of dynamic positioning (DP) systems for marine vessels. Common observer types used in DP today include model-based designs such as the nonlinear passive observer (NPO), see Fossen and Strand (1999), or an exteded Kalman filter, see Sørensen (2011) for an overview and the references therein. For other examples of implementation in DP see for instance Tannuri and Morishita (2006) and Hassani et al. (2013). These observers are based on a kinetic model of the vessel, and use position measurements from e.g. Global Navigation and Sensor Systems (GNSS), hydro-acoustic, laser, or microwaves, to reconstruct unmeasured states, filter out wave frequency motions, estimate bias, and in case of signal loss, do dead reckoning.

Signal-based, or kinematic, observers are also recently proposed for DP applications. These do not contain model parameters nor vessel-specific information, in contrast to model-based observers. In general, the methods integrate acceleration and angular rate measurements from inertial measurement units (IMU) to compute position and attitude estimates, correcting the estimates from drifting using position and compass (or magnetometer) measurements. Gravity and gyro bias are also compensated. For details see e.g. Grip et al. (2012), Grip et al. (2015) and Bryne et al. (2015).

The observers mentioned here assume in the design that the measurements are available continuously, which is not the case in reality. This was addressed in Brodtkorb et al. (2015), where measurements of position, velocity and acceleration were fused in a hybrid signal-based observer. The observer design was based on the assumption that position and velocity measurements were available only sporadically, and used acceleration measurement available at a high rate for position prediction. On a similar note, Ferrante et al. (2016) considers state estimation of linear systems where the measurements are available sporadically. The work considers systems where data used for control is transmitted over networks, where data can get lost or is available intermittently.

This paper extends the observer from Brodtkorb et al. (2015) to the more realistic case where no linear velocity and angular acceleration measurements are available. The observer error dynamics are shown uniformly globally asymptotically stable (UGAS) by using theory from hybrid dynamical systems as described in Goebel et al. (2012) and cascaded systems. The observer is tested in simulations of a marine surface vessel conducting DP operations.

The paper is organized as follows: Section 2 introduces the mathematical model and available measurements used for the observer design. The observer is designed in Section 3, and stability is discussed in Section 4. The observer is

⋆ This work was supported by the Research Council of Norway through the Centres of Excellence funding scheme, project number 23254 - NTNU AMOS, and in part by NSF grant number ECCS-1508757 and AFOSR grant number FA9550-15-1-0155.

tested in simulations of a surface vessel in DP in Section 5, and Section 6 concludes the paper.

2. MATHEMATICAL MODELING

Two reference frames are used thoughout this paper. The North-East-Down (NED) frame is a local Earth-fixed reference frame with origin at the mean free surface, and the second reference frame is a body-fixed frame. The NED frame is assumed inertial.

2.1 Marine Vessel Modeling

The signal-based observer is based on the kinematic (strapdown) equations relating position, velocity and acceleration of the vessel. Here, we are looking only at motions in the horizontal plane, so we only consider surge, sway and yaw motions [1]. The equations of motion are

$$\dot{p} = R(\psi)v \tag{1a}$$
$$\dot{\psi} = r \tag{1b}$$
$$\dot{v} = a \tag{1c}$$

where p is the position vector in north and east, v is the body-fixed surge and sway velocity vector, a is the body-fixed surge and sway acceleration vector, ψ is the heading angle, and r is the yaw rate. Throughout this paper the rotation matrix $R(\psi)$ refers to the 2×2 rotation matrix given by

$$R(\psi) = \begin{bmatrix} \cos(\psi) & -\sin(\psi) \\ \sin(\psi) & \cos(\psi) \end{bmatrix}. \tag{2}$$

2.2 Measurements

DP vessels have statutory class requirements on the onboard instrumentation, and system redundancy. Vessels have positioning systems, e.g. GNSS, acoustics, or laser, a compass measuring heading angle, and inertial measurement units (IMU) that combine gyroscopes for measuring angular rates and accelerometers for measuring linear acceleration. The measurements are taken at different sampling rates ranging from 0.1-2 Hz for acoustics, 0.5-4 Hz for GNSS position measurements, to 100-200 Hz for IMU angular velocity and acceleration measurements.

We assume to have measurements of position $p = [N\ E]^\top$ and heading ψ with non-constant sample time in the interval $[T_{min}, T_{max}]$, where $0 < T_{min} \leq T_{max}$. The yaw rate r, and linear acceleration a are assumed to be measured at a high rate, approximated as continuous sampling. We also assume that r and a are bounded. Notice that we do not have linear velocity or angular acceleration measurements available. Noise on the measurements is not considered in the stability analysis, but is included in the simulations.

For convenience we constrain the system states to a compact set $\mathcal{K}$, $(p, \psi, v) \in \mathcal{K} \subset \mathbb{R}^5$. The observer design does not depend on this set.

[1] Since we are considering only surge, sway and yaw motion, the coupling effects in roll and pitch are neglected, as well as the effect of gravity.

3. HYBRID OBSERVER

A hybrid observer is designed based on (1) by utilizing the measurements when they are available. The observer states, denoted $(\cdot)_i$, flow with the yaw rate and linear acceleration measurements, and are updated with the occasional position and heading measurements. To mitigate the effect of position and compass measurement noise, multiple copies of position, heading and velocity are saved in the observer and averaged. The position, heading, and velocity estimates are

$$\hat{p} := \frac{1}{N}\sum_{i=1}^{N} p_i, \quad \hat{\psi} := \frac{1}{N}\sum_{i=1}^{N} \psi_i, \quad \hat{v} := \frac{1}{N}\sum_{i=1}^{N} v_i \tag{3}$$

where p_i, $i = \{1, ..., N\}$ are the north and east position states in the observer, ψ_i are the heading states, and v_i are the linear velocity states. The observer states flow as

$$\dot{p}_i = R(\hat{\psi})v_i \tag{4a}$$
$$\dot{\psi}_i = r \tag{4b}$$
$$\dot{v}_i = a \tag{4c}$$
$$\dot{M} = R(\hat{\psi}) \tag{4d}$$
$$\dot{\tau} = -1, \tag{4e}$$

with $i = \{1, ..., N\}$ copies of position, heading and velocity flow with the available yaw rate r and acceleration measurement a. The states are allowed to flow when

$$\begin{aligned} &((p, \psi, v), (p_1, \psi_1, v_1), ..., (p_N, \psi_N, v_N), M, \tau) \in C \\ &C := \mathcal{K} \times (\mathbb{R}^2 \times \mathbb{R}^1 \times \mathbb{R}^2)^N \\ &\quad \times \left\{P \in \mathbb{R}^{2\times 2} : ||P||_2 \leq T_{max}\right\} \times [0, T_{max}]. \end{aligned} \tag{5}$$

In particular M belongs to the set of 2×2 matrices with induced 2 norm less than or equal to T_{max}, see Section 4.3 for details. The observer flows in between position and compass measurement times, when $\tau \in [0, T_{max}]$. A new position and compass measurement is available with non-constant sampling time with at least T_{min} seconds between samples and at most T_{max} seconds. Hence a jump is triggered when $\tau = 0$, with the jump dynamics

$$p_i^+ = p_{i-1} \tag{6a}$$
$$\psi_i^+ = \psi_{i-1} \tag{6b}$$
$$v_i^+ = v_i + \kappa M^{-1}(p_i - p_{i-1}), \tag{6c}$$
$$M^+ = 0, \tag{6d}$$
$$\tau^+ \in [T_{min}, T_{max}], \tag{6e}$$

with $i = \{1, .., N\}$ and the measurements $p_0 := p$ and $\psi_0 := \psi$. The measurements of position and heading are saved into the first observer states (p_1, ψ_1), and the remainder of the states are shifted one place back in the shift register. The velocity states are updated with the state itself, and a correction term consisting of a gain κ, the inverse of the matrix M involving the rotation matrix integrated over time, and the error between position states i and $i-1$. The jump set is

$$\begin{aligned} &((p, \psi, v), (p_1, \psi_1, v_1), ..., (p_N, \psi_N, v_N), M, \tau) \in D \\ &D := \mathcal{K} \times (\mathbb{R}^2 \times \mathbb{R}^1 \times \mathbb{R}^2)^N \\ &\quad \times \left\{P \in \mathbb{R}^{2\times 2} : ||P||_2 \leq T_{max},\ \det(P) \geq \rho\right\} \times \{0\}. \end{aligned} \tag{7}$$

The observer has two parameters; κ in (6c), which can be anything in $(-2, 0)$, and $\rho > 0$ in (7) which ensures that $\det(M)$ is larger than zero so that M is invertible during jumps. This last constraint is related to making sure that

the system is observable with the available measurements. The yaw dynamics are usually slow compared to the sampling period, and this makes it less likely to encounter det(M)=0. The parameter ρ should be small to allow for as many signals ψ as possible.

4. STABILITY

We are using Lyapunov results for hybrid systems (Goebel et al., 2012), and cascaded systems to prove that the observer error dynamics has the origin uniformly globally asymptotically stable (UGAS).

We are analyzing stability of the plant (1) with the observer given in (4) and (6), with the flow set (5) and the jump set (7). The set for which we are analyzing stability is

$$\begin{aligned}\mathcal{A} :=\{&((p,\psi,v),(p_1,\psi_1,v_1),...,(p_N,\psi_N,v_N),M,\tau)\in C:\\ &p_i=p,\ \psi_i=\psi,\ v_i=v,\ \forall i\in\{1,...,N\}\}.\end{aligned} \tag{8}$$

Theorem 1: If $\kappa \in (-2, 0)$ and $\rho > 0$ then the set $\mathcal{A}$ in (8) is UGAS for the hybrid system consisting of the plant (1) the observer given in (4) and (6), with flow set (5) and jump set (7). □

The proof is done sequentially in the next sections. The observer error dynamics are first introduced. The heading error dynamics are shown UGAS, and the observer error dynamics for $N = 1$ without including heading are shown UGAS by applying a coordinate transformation. Lastly the analysis for the observer error dynamics for $N > 1$ follows from the case where $N = 1$ by using cascade theory.

4.1 Error Dynamics

Define the error states as:

$$\begin{aligned}e_i &= p_i - p_{i-1},\\ y_i &= \psi_i - \psi_{i-1},\\ z_i &= v_i - v_{i-1},\end{aligned}$$

for all $i \in \{1, .., N\}$, with the actual states of the system $p_0 := p,\ \psi_0 := \psi,$ and $v_0 := v$. The relationship between the velocity and position is $\dot{p}_0 = R(\psi_0)v_0$. Write the observer error dynamics as:

$$\dot{e}_i = \begin{cases} R(\hat{\psi})z_i + [R(\hat{\psi}) - R(\psi)]v & i = 1\\ R(\hat{\psi})z_i & i \in \{2,\dots,N\}\end{cases} \tag{9a}$$

$$\dot{z}_i = 0 \qquad i \in \{1,\dots,N\} \tag{9b}$$

$$\dot{M} = R(\hat{\psi}) \tag{9c}$$

$$\dot{\tau} = -1 \tag{9d}$$

$$e_i^+ = e_{i-1} \qquad i \in \{1,\dots,N\} \tag{9e}$$

$$z_i^+ = z_i + \kappa M^{-1} e_i \qquad i \in \{1,\dots,N\} \tag{9f}$$

$$M^+ = 0 \tag{9g}$$

$$\tau^+ \in [T_{min}, T_{max}], \tag{9h}$$

with position error $e_0 := p - p = 0$. Note that when the heading estimate has converged, $\hat{\psi} = \psi$, the extra term for $i = 1$ in (9a) disappears. The heading error dynamics are:

$$\dot{y}_i = 0 \qquad i \in \{1,\dots,N\} \tag{10a}$$

$$y_i^+ = y_{i-1} \qquad i \in \{1,\dots,N\}, \tag{10b}$$

with heading error $y_0 := \psi - \psi = 0$.

4.2 Heading Error Analysis

The heading error dynamics are independent of the other states, and is input to the flow dynamics of position via M.

Claim 1: The origin of the heading error dynamics (10) with states y_i are UGAS. □

Proof: The proposed Lyapunov function candidate is

$$V(y,\tau) := \exp(L\tau)\sum_{i=1}^{N} k_i y_i^\top y_i \tag{11}$$

$L > 0$, and with weights k_i chosen so that

$$k_i > \exp(LT_{max})k_{i+1},\ i \in \{1,...,N\}$$

with $k_{N+1} := 0$. The Lyapunov function $V(y,\tau)$ can be lower bounded by choosing $\tau = 0$ and upper bounded by choosing $\tau = T_{max}$. The time derivative of V along the trajectories of the state, and the difference between V before and after a jump are

$$\begin{aligned}\langle \nabla V(y,\tau), f\rangle &= \exp(L\tau)\left(L\dot{\tau}\sum_{i=1}^{N} k_i y_i^\top y_i + 2\sum_{i=1}^{N} k_i y_i^\top \dot{y}_i\right)\\ &= -LV(y,\tau).\end{aligned}$$

$$\begin{aligned}&V(y^+,\tau^+) - V(y,\tau)\\ &\qquad \le \exp(LT_{max})\sum_{i=1}^{N} k_i y_{i-1}^\top y_{i-1} - \sum_{i=1}^{N} k_i y_i^\top y_i\end{aligned}$$

$y_0 = \psi - \psi = 0$, so the first sum can be contracted.

$$\begin{aligned}&V(y^+,\tau^+) - V(y,\tau)\\ &\qquad \le \exp(LT_{max})\sum_{i=2}^{N} k_i y_{i-1}^\top y_{i-1} - \sum_{i=1}^{N} k_i y_i^\top y_i\\ &\qquad \le \exp(LT_{max})\sum_{i=1}^{N-1} k_{i+1} y_i^\top y_i - \sum_{i=1}^{N} k_i y_i^\top y_i\\ &\qquad \le \sum_{i=1}^{N} \left(\exp(LT_{max})k_{i+1} - k_i\right) y_i^\top y_i\end{aligned}$$

Due to the definition of $k_i\ \forall i$, the terms in the first sum can be dominated by the terms in the second sum. Then there exists a $\delta > 0$ such that

$$V(y^+,\tau^+) - V(y,\tau) \le -\delta y^\top y.$$

□

4.3 Lyapunov Analysis for $N = 1$

Assume that $\hat{\psi}$ has converged to ψ, so that $R(\hat{\psi}) - R(\psi) = 0$.

Claim 2: Given that $\hat{\psi} = \psi$, the origin of the observer error dynamics given by (9) is UGAS. □

Proof: We introduce new coordinates

$$\begin{aligned}x_1 &:= e_1 - Mz_1\\ x_2 &:= z_1,\end{aligned} \tag{12}$$

and rewrite the error dynamics as

$$\dot{x}_1 = 0 \tag{13a}$$
$$\dot{x}_2 = 0 \tag{13b}$$
$$\dot{\tau} = -1 \tag{13c}$$
$$x_1^+ = 0 \tag{13d}$$
$$x_2^+ = (1+\kappa)x_2 + \kappa M^{-1}x_1 \tag{13e}$$
$$\tau^+ \in [T_{min}, T_{max}]. \tag{13f}$$

Choose the following Lyapunov function candidate:

$$V(x,\tau) := \exp(\mu\tau)(\ell x_1^\top x_1 + x_2^\top x_2) \tag{14}$$

with $0 < \mu \ll 1$, and a large number ℓ. The time derivative of V along the trajectories of (x,τ) is

$$\begin{aligned}\langle \nabla V(x,\tau), f(x,\tau)\rangle &= -\mu V(x,\tau) + 2\exp(\mu\tau)\left(x_1^\top \dot{x}_1 + x_2^\top \dot{x}_2\right)\\ &= -\mu V(x,\tau).\end{aligned}$$

Before investigating what happens during jumps, we calculate a convenient bound on $V(x^+,\tau^+) - V(x,\tau)$ using the induced 2 norm of M^{-1}

$$||M^{-1}||_2 = \frac{||M||_2}{\det(M)},$$

where $\det(M)$ is the determinant of M. The induced 2 norm of a matrix is defined as

$$||M||_2 := \max_{|v|_2=1} |Mv|_2,$$

with the vector norm $|v|_2 = 1$. In this case M evolves as $\dot{M}(t) = R(\hat{\psi}(t))$ with initial condition $M(0) = 0$. The induced 2 norm of M is computed in the following:

$$\begin{aligned}|M(t)v|_2 &= \left|\int_0^t R(\hat{\psi}(s))ds\ v\right|_2\\ &\le \int_0^t \left|R(\hat{\psi}(s))v\right|_2 ds.\end{aligned}$$

Use that $R(\hat{\psi}(s))$ is a rotation matrix for all s, so it rotates v, not altering the magnitude of the vector.

$$\begin{aligned}|M(t)v|_2 &\le \int_0^t |v|_2\, ds\\ &\le \int_0^t ds = t \le T_{max},\end{aligned}$$

so $||M||_2 \le T_{max}$. The determinant of M cannot be smaller than ρ in the jump map, so we get that

$$||M^{-1}||_2 \le \frac{T_{max}}{\rho}.$$

During jumps we get

$$\begin{aligned}V(x^+,\tau^+) - V(x,\tau) &\le \exp(\mu T_{max})[(1+\kappa)x_2 + \kappa M^{-1}x_1)^\top\\ &\quad ((1+\kappa)x_2 + \kappa M^{-1}x_1] - \ell x_1^\top x_1 - x_2^\top x_2\\ &\le \exp(\mu T_{max})[(1+\kappa)^2 x_2^\top x_2 + \kappa^2 x_1^\top (M^{-1})^\top M^{-1} x_1\\ &\quad + 2\kappa(1+\kappa)x_1^\top (M^{-1})^\top x_2] - \ell x_1^\top x_1 - x_2^\top x_2\\ &\le \exp(\mu T_{max})[(1+\kappa)^2 x_2^\top x_2 + \kappa^2 \frac{T_{max}^2}{\rho^2} x_1^\top x_1\\ &\quad + 2(1+\kappa)\kappa \frac{T_{max}}{\rho} x_1^\top x_2] - \ell x_1^\top x_1 - x_2^\top x_2.\end{aligned}$$

We use Young's inequality for completion of squares

$$2a^\top b \le \frac{1}{\varepsilon} a^\top a + \varepsilon b^\top b, \qquad \forall \varepsilon > 0.$$

By choosing $a = \kappa \frac{T_{max}}{\rho} x_1$, and $b = (1+\kappa)x_2$, we get

$$\begin{aligned}&V(x^+,\tau^+) - V(x,\tau)\\ &\quad \le \left[\exp(\mu T_{max})\left(\kappa^2 \frac{T_{max}^2}{\rho^2} + \kappa^2 \frac{T_{max}^2}{\rho^2}\frac{1}{\varepsilon}\right) - \ell\right] x_1^\top x_1\\ &\quad + \left[\exp(\mu T_{max})\left((1+\kappa)^2 + (1+\kappa)^2\varepsilon\right) - 1\right] x_2^\top x_2\end{aligned}$$

The Lyapunov function decreases during jumps if

$$\ell > \exp(\mu T_{max})\kappa^2 \frac{T_{max}^2}{\rho^2}\left(1 + \frac{1}{\varepsilon}\right) \tag{15a}$$
$$1 > \exp(\mu T_{max})(1+\kappa)^2(1+\varepsilon). \tag{15b}$$

When $\mu = 0$ and $\varepsilon = 0$ (15b) holds since $\kappa \in (-2, 0)$. By continuity it still holds for $\mu > 0$ and $\varepsilon > 0$ sufficiently small. After picking such a $\mu > 0$ and $\varepsilon > 0$, we choose ℓ to satisfy (15a).

We can bound the Lyapunov function given in (14) with the original states (e_1, z_1) by noting that

$$\begin{aligned}V(x,\tau) &\le \ell \exp(\mu T_{max}) \left|\begin{bmatrix} x_1 \\ x_2 \end{bmatrix}\right|^2\\ &\le \ell \exp(\mu T_{max})(1+T_{max})^2 \left|\begin{bmatrix} e_1 \\ z_1 \end{bmatrix}\right|^2,\end{aligned} \tag{16}$$

and

$$\begin{aligned}V(x,\tau) &\ge \left|\begin{bmatrix} x_1 \\ x_2 \end{bmatrix}\right|^2\\ &= \frac{(1+T_{max})^2}{(1+T_{max})^2}\left|\begin{bmatrix} x_1 \\ x_2 \end{bmatrix}\right|^2\\ &\ge \frac{1}{(1+T_{max})^2}\left|\begin{bmatrix} e_1 \\ z_1 \end{bmatrix}\right|^2.\end{aligned} \tag{17}$$

By Theorem 3.18 Goebel et al. (2012) the set $\mathcal{A}$ in (8) is globally asymptotically stable for (9) with $\hat{\psi} = \psi$ and $N = 1$ given that (15) holds. □

4.4 Lyapunov Analysis for $N > 1$

When $N > 1$ there are two considerations we have to take. Firstly, the flow dynamics get an extra term when the heading estimate is not equal to the actual heading, and secondly, the position estimates $e_{i-1},\ i = \{2, ..., N\}$ in the jump dynamics are not zero.

Flow Dynamics with $\hat{\psi} \neq \psi$ When $\hat{\psi}$ has not converged to ψ yet, we are left with an extra term in the position error dynamics of e_1. Using (12), the error dynamics are

$$\dot{x}_1 = [R(\hat{\psi}) - R(\psi)]v \tag{18a}$$
$$\dot{x}_2 = 0 \tag{18b}$$
$$\dot{\tau} = -1 \tag{18c}$$
$$x_1^+ = 0 \tag{18d}$$
$$x_2^+ = (1+\kappa)x_2 + \kappa M^{-1}x_1 \tag{18e}$$
$$\tau^+ \in [T_{min}, T_{max}] \tag{18f}$$

The rotation matrix is bounded for all $\hat{\psi}$ and ψ, and the velocity v is bounded, since it is contained in the compact set $\mathcal{K}$. The jump dynamics are unchanged.

Claim 3: The system given by (18) with input v is input-to-state stable (ISS). □

Proof (from the proof of Proposition 2.7, Cai and Teel (2009)): The Lyapunov function $V(x,\tau)$ in (14) is bounded by two κ_∞-functions in (17). Furthermore, we get the time derivative along the state trajectories

$$\begin{aligned}&\langle \nabla V(x,\tau), f(x,\tau)\rangle \\ &\quad \leq -\mu V(x,\tau) + 2\exp(\mu\tau)\ell x_1^\top [R(\hat{\psi}) - R(\psi)]v,\end{aligned}$$

where the first term is from the unperturbed e_1 dynamics, and the second term is due to the difference $\hat{\psi} - \psi$. Using Young's inequality for completion of squares with $a = \sqrt{\ell}x_1$ and $b = 2\sqrt{\ell}\exp(\mu\tau)[R(\hat{\psi}) - R(\psi)]v$, we get

$$\begin{aligned}&\langle \nabla V(x,\tau), f(x,\tau)\rangle \\ &\quad \leq -\mu V(x,\tau) + \frac{1}{2}\mu\ell x_1^\top x_1 + \frac{1}{2\mu}\ell\exp(2\mu T_{max})(2|v|)^2 \\ &\quad \leq -\frac{1}{2}\mu V(x,\tau) + \alpha_1(|v|).\end{aligned}$$

We know that $V(x,\tau)$ can be lower bounded as in (17), and $\alpha_1(s) := \frac{2}{\mu}\ell\exp(2\mu T_{max})s^2$, $\forall s \geq 0$ is a class κ-function since $\alpha_1(0) = 0$ and it is strictly increasing. Then the Lyapunov function $V(x,\tau)$ in (14) is an ISS-Lyapunov function w.r.t the input v, and the hybrid system (18) is ISS w.r.t. v. □

Theorem 2: Given that $\kappa \in (-2, 0)$ and (15) holds, the origin of the cascaded system (18) and (10) is UGAS. □

The proof follows from Goebel et al. (2009) Corollary 19. Consider the hybrid system $\mathcal{H} = (C, F, C, G)$ consisting of the position and velocity error dynamics (18) and the heading error dynamics (10). The compact set

$$\begin{aligned}\mathcal{A}_1 =\{&((p,\psi,v),(p_1,\psi_1,v_1),...,(p_N,\psi_N,v_N),M,\tau) \in C : \\ &p_i = \beta\mathbb{B},\ \psi_i = \psi,\ v_i = \beta\mathbb{B},\ \forall i \in \{1,...,N\}\},\end{aligned}$$

with $\beta > 0$ and $\mathbb{B}$ the unit ball is globally pre-asymptotically stable (GpAS) for $\mathcal{H}$ (Claim 1). Further, the compact set $\mathcal{A}$ from (8), which is a subset of $\mathcal{A}_1$ is GpAS for $\mathcal{H}|_{\mathcal{A}_1} := (C \cap \mathcal{A}_1, F, D \cap \mathcal{A}_1, G \cap \mathcal{A}_1)$ (Claim 2). Then set $\mathcal{A}$ in (8) is UGAS for $\mathcal{H}$, given by (18) and (10). □

Jump Dynamics with $e_{i-1} \neq 0$ Again, we assume that $\hat{\psi} = \psi$ so that $R(\hat{\psi}) - R(\psi) = 0$. In general, the system (9) with $i = \{1,...,N\}$ can be written as

$$\dot{e}_i = R(\hat{\psi})z_i \tag{19a}$$
$$\dot{z}_i = 0 \tag{19b}$$
$$\dot{M} = R(\hat{\psi}) \tag{19c}$$
$$e_i^+ = e_{i-1} \tag{19d}$$
$$z_i^+ = z_i + \kappa M^{-1}e_i \tag{19e}$$
$$M^+ = 0. \tag{19f}$$

In Section 4.3 the case with $N = 1$ was proved. The error dynamics for $i \in \{2,...,N\}$ are identical to the case where $N = 1$, except for the position error jumps $e_i^+ = e_{i-1}$, in stead of $e_1^+ = 0$.

Claim 4: Assuming that $\hat{\psi} = \psi$, the system given by (19) with input e_{i-1} is ISS, implying that the origin of the unforced system (19) with $e_{i-1} = 0$ is UGAS. □

Proof: The position jump dynamics changes the x_1 jump dynamics in (13d), which adds an extra term in the Lyapunov function during jumps. The flow dynamics are unchanged. The change in the $V(x,\tau)$ in (14) can be written as

$$\begin{aligned}&V(x^+,\tau^+) - V(x,\tau) \\ &\quad \leq -\gamma_1 x_1^\top x_1 - \gamma_2 x_2^\top x_2 + \exp(\mu T_{max})\ell e_{i-1}^\top e_{i-1} \\ &\quad \leq -\alpha_2(|x|) + \alpha_3(|e_{i-1}|),\end{aligned}$$

where $\alpha_2(|x|)$ is a class κ_∞-function given that (15) holds, and $\alpha_3(|e_{i-1}|)$ is a class κ-function. It follows that $V(x,\tau)$ (14) is an ISS-Lyapunov function for (19), then the system (19) is ISS with respect to the input e_{i-1} (Cai and Teel, 2009, Proposition 2.7). □

5. SIMULATION RESULTS AND DISCUSSION

The observer was implemented in MATLAB/Simulink, and simulated with a platform supply vessel in DP. The vessel has length 80 meters and breadth 17.4 meters. The control objective was to control the vessel to the desired time-varying reference $p_d(t)$ with the desired velocity trajectory $v_d(t)$:

$$\lim_{t\to\infty} p(t) - p_d(t) = 0$$
$$\lim_{t\to\infty} v(t) - v_d(t) = 0.$$

A nonlinear proportional, integral, derivative (nPID) controller was used to achieve trajectory tracking using output feedback, with current as the only environmental force. The current speed was $[-0.3\ 0.5]$ m/s in the North-East frame. Realistic noise values were used, where the position noise variance σ_p^2 was varied in the simulations.

Figures 1 and 2 show the actual and estimated north position and surge velocity for different values of N when the vessel changes setpoint and heading several times. At 200 seconds the vessel starts changing to the first setpoint; 3 m north, -5 m east, and with a heading of $-90°$. At 500 seconds the vessel does a new setpoint change to -2 m north, 5 m east, and heading angle $-60°$. The observer performance in the other degrees of freedom was comparable to the north position and surge velocity.

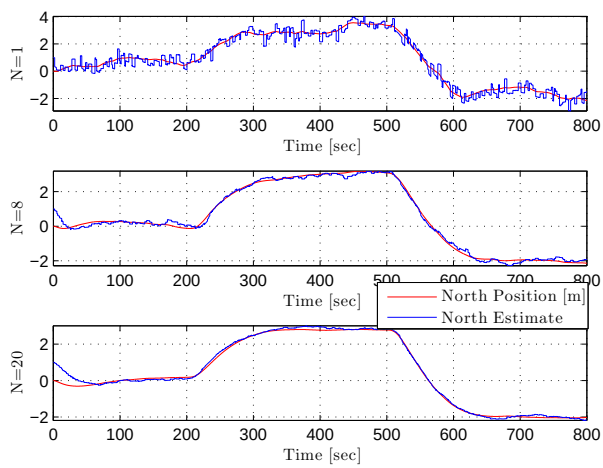

Fig. 1. Position and estimated position, for $N = 1, N = 8$ and $N = 20$. $T_{min} = 1$ $T_{max} = 5$ with noisy measurements $\sigma_p^2 = 0.3^2$ and estimates in feedback.

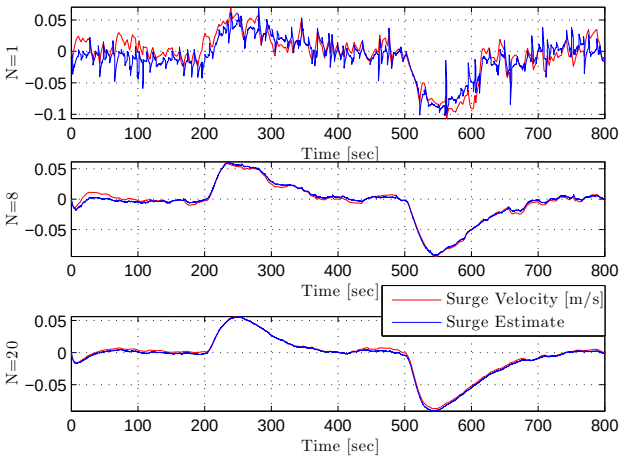

Fig. 2. Velocity and estimated velocity, for $N = 1, N = 8$ and $N = 20$. $T_{min} = 1$ $T_{max} = 5$ with noisy measurements $\sigma_p^2 = 0.3^2$ and estimates in feedback.

The observer states were initialized as $p_i = 1$ m, $\psi_i = 1°$ and $v_i = 0$ m/s, with the vessel states all starting at zero. It is clear from Figure 1 that as the number of states in the observer increases, the variance on the estimates decreases. Table 1 shows the variance for $N = 1$, $N = 8$, and $N = 20$. The estimation error also decreases for increasing N, and the overall reference tracking performance increases when the estimates are less oscillatory. The performance is similar for $N = 8$ and $N = 20$, with a longer initialization phase for $N = 20$ and some induced oscillations on the position for $N = 8$. Decreasing N and T_{max} decreases the convergence time greatly since $p_i - p_{i-1}$ is used as correction term in the velocity update dynamics. It was also found that with higher noise variance, the effect of increasing N was greater.

	Position variance [m^2]	Velocity variance [m^2/s^2]
$N = 1$	0.1016	$6.53 \cdot 10^{-5}$
$N = 8$	0.0162	$1.34 \cdot 10^{-5}$
$N = 20$	0.0030	$1.21 \cdot 10^{-5}$

Table 1. Variance of the estimates with $T_{min} = 1$ $T_{max} = 5$, and $\sigma_p^2 = 0.3^2$

The velocity estimates in Figure 2 were also better for larger N. The best velocity estimates were achieved by choosing κ just large enough so the velocity estimates did not drift. In particular for $N = 1$, $\kappa = -0.08$, for $N = 8, \kappa = -0.03$, and for $N = 20, \kappa = -0.02$. In general it was found that for increasing N, the value of κ could beneficially be decreased slightly. Without noise $\kappa = -1$ provided perfect position and velocity estimation.

The velocity dynamics were sensitive to position noise. For high position noise variance, small feedback gain on velocity produced less oscillatory estimates, but too low gain caused the velocity estimates to drift. Increasing N improved the estimation. The frequency of the position updates also influences the choice of κ, see (15). With frequent position measurements, κ could be chosen smaller, and vice versa in the simulations.

6. CONCLUSION

The signal-based observer without velocity and angular acceleration measurements updates worked well in simulations with and without measurement noise. Having a large number of states N in the observer was beneficial to mitigate noise with large variance.

For future work, rigorously analyzing the effect of the noise in the position and compass measurements is of interest. In addition, we may consider extending the velocity update dynamics to the case where M is not necessarily invertible at every sampling time.

REFERENCES

Brodtkorb, A., Teel, A., and Sørensen, A.J. (2015). Sensor-based hybrid observer for dynamic positioning. *Proceedings of the IEEE Conference on Decision and Control*, 2015-December, 948–953.

Bryne, T., Fossen, T., and Johansen, T. (2015). A virtual vertical reference concept for GNSS/INS applications at the sea surface. *IFAC Proceedings Volumes (IFAC-PapersOnline)*, 48(16), 127–133.

Cai, C. and Teel, A. (2009). Characterizations of input-to-state stability for hybrid systems. *Systems and Control Letters*, 58(1), 47–53.

Ferrante, F., Gouaisbaut, F., and Sanfelice, R.G. (2016). State estimation of linear systems in the presence of sporadic measurements. *To appear in: Automatica*.

Fossen, T.I. and Strand, J.P. (1999). Passive nonlinear observer design for ships using Lyapunov methods: full-scale experiments with a supply vessel. *Automatica*, 35(1), 3 – 16.

Goebel, R., Sanfelice, R., and Teel, A.R. (2009). Hybrid dynamical systems robust stability and control for systems that combine continuous-time and discrete-time dynamics. *IEEE Control Systems Magazine, April 2009*, 28–93.

Goebel, R., Sanfelice, R.G., and Teel, A.R. (2012). *Hybrid Dynamical Systems, Modelling, Stability and Robustness*. Princeton University Press.

Grip, H.F., Fossen, T.I., Johansen, T.A., and Saberi, A. (2012). Attitude estimation using biased gyro and vector measurements with time-varying reference vectors. *IEEE Transactions on Automatic Control*, 57(5), 1332–1338.

Grip, H.F., Fossen, T.I., Johansen, T.A., and Saberi, A. (2015). Globally esponentially stable attitude and gyro bias estimation with application to GNSS/INS integration. *Automatica*, 51, 158–166.

Hassani, V., Sørensen, A.J., and Pascoal, A.M. (2013). A novel methodology for robust dynamic positioning of marine vessels: Theory and experiments. *Proceedings of the American Control Conference*, 560–565.

Sørensen, A.J. (2011). A survey of dynamic positioning control systems. *Annual Reviews in Control*, 35(1), 123–136.

Tannuri, E.A. and Morishita, H.M. (2006). Experimental and numerical evaluation of a typical dynamic positioning system. *Applied Ocean Research*, 28(2), 133–146.